TEMPORAL AND LONGITUDINAL VARIANCES IN WOOD LOG CROSS-SECTION IMAGE ANALYSIS

Rudolf Schraml [a] *Johann Charwat-Pessler* [b] *Andreas Uhl* [a]

[a] University of Salzburg, Jakob Haringer Str. 2, 5020 Salzburg, Austria
[b] University of Applied Sciences Salzburg, Markt 136a, 5431 Kuchl, Austria

ABSTRACT

In this work two practical issues of biometric log recognition using log end images are investigated: Temporal and longitudinal variances of log cross-sections (CSs). These variances are related to the requirement of robustness for biometric characteristics. A texture feature-based fingerprint matching technique is used to compute matching scores between CS images. Our experimental evaluation is based on the temporal and longitudinal variances of 35 slices of a single tree log which where captured at four time delayed sessions. Results indicate, that biometric log recognition using log end images is robust and is able to overcome both issues. This work contributes to the development of a biometric log recognition system by showing that a texture feature-based matching technique is applicable to log CSs.

Index Terms— Biometric log traceability, Cross-section analysis, Texture feature-based matching technique

1. INTRODUCTION

Traceability of wood logs is a basic requirement to manage economical and social issues. In economic terms, traceability of wood logs is required to map the ownership structure of each log. Due to the ecological rethinking social aspects like sustainability have become more important. So-called wood certificates like the Pan European Forest Certification (PEFC) are based on traceability and are a must have for all end-sellers.

Currently, log traceability is established by physically marking each log (see [1]). State-of-the-art systems propose the usage of Radio Frequency Identification (RFID) to reach traceability from forest site to further processing companies (see [2],[3]). Another idea relies on biometric recognition of wood logs. In the works of [4],[5],[6],[7],[8] approaches to establish biometric log traceability within the sawmill were presented. The approaches presented in [4],[5],[7] utilized 2D and 3D scanners to extract geometric wood properties. In [6],[8] a computer tomography scanner was used to extract knot positions to enable traceability between logs and the cut boards. Due to low recognition rates, these approaches are not applicable for industrial usage within the sawmill and are even less suitable to deal with the increasing variety of trees at forest site. Furthermore, the utilized capturing devices are expensive and not applicable in the forest based industries.

Similar as for human fingerprint recognition, we assume that annual ring patterns of log ends can be used to recognize wood logs. Log end images can be captured by digital cameras at forest site and processing companies. This work contributes to the development of a biometric log recognition approach using log end images by investigating two practical issues: Temporal and longitudinal variances of cross-sections (CSs) in wood logs. For human biometrics, robustness of the utilized biometric characteristic is a basic requirement. In case of CSs robustness is related to the temporal changes caused by environmental conditions and the longitudinal variations of the CS pattern within a tree log. Temporal changes are caused by light and humidity and result in deformations like cracks and discolourations. Longitudinal variations result from log end cutting or from capturing different log ends.

For our investigations the FingerCode approach by [9], [10] is adopted to CS images. Additionally, a Log-Gabor extension of the fingerprint enhancement approach by [11] is utilized to enhance the annual ring pattern. Thus, our work additionally sheds light on the general applicability of texture features for CS matching. For the experimental evaluation 35 slices of a single log are utilized. Each slice was captured four times at time-delayed sessions. This testset enables the computation of the temporal variances between time-delayed sessions from each cross-section slice. Longitudinal variances are computed among the CS images of the 35 slices of the testset.

At, first Section 2 introduces the computation and matching of Gabor-based features from CS images. The experimental setup and results are presented in Section 3 followed by the conclusion in Section 4.

2. CROSS-SECTION CODES (CS-CODES)

The CS-Code computation is based on the FingerCode approach proposed in [9] and [10]. This technique utilizes

THIS WORK IS PARTIALLY FUNDED BY THE AUSTRIAN SCIENCE FUND (FWF) UNDER PROJECT NO. TRP-254.

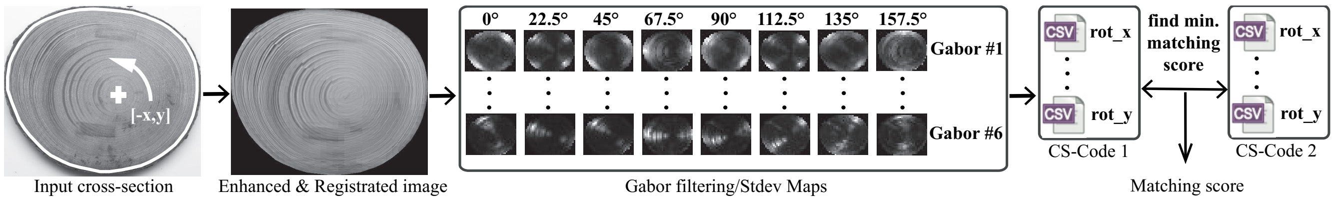

Fig. 1: CS-Code computation and matching scheme

a Gabor-based descriptor which extracts local ridge orientations of a fingerprint. In the next section the CS image registration & enhancement procedure is considered in detail. Subsequently, in Section 2.2 the CS-Code computation and the matching procedure between CS-Codes extracted from different CS images is outlined.

2.1. Cross-section registration & enhancement

Due to cutting disturbances annual ring enhancement is a crucial task for any subsequent feature extraction procedure. As opposed to human fingerprints, the frequency of the annual ring pattern is strongly varying. Our enhancement procedure is based on the fingerprint enhancement approach presented in [11]. CS registration is performed in three steps. The left image in Fig. 1 shows an example for an input CS image. The CS border and the pith position have to be determined in advance (see [12],[13]). For image registration the image is rotated around the pith position, cropped to the CS bounding box and finally scaled to 512 pixels in width. Rotation can be performed to generate rotated versions of each CS image or to align the CS to a unique position (eg. according to the center of mass). For CS image enhancement the CS is subdivided in half/ non-overlapping blocks (eg. 16x16 pixels). Enhancement is performed in three consecutive stages: Local orientation estimation, local frequency estimation and adaptive filtering.

At first, for each block principal component analysis of the local Fourier Spectrum is performed to determine its local orientation (see [12]). Commonly, CSs are disturbed due to cutting. Thus, wrong orientations are slightly corrected by low-pass filtering the local orientation field with a Gaussian filter. Next, for each block and its local orientation the dominant frequency is determined. For this purpose, the local Fourier Spectrum of each block is subdivided into subbands and sectors. The dominating frequency of a block is determined by summing up all frequency magnitudes in each sector subband. It is assumed that the maximum sector-subband represents the dominating frequency. If the maximum sector does not correspond to the block orientation the result is neglected. In a further step for each neglected value the local frequency is interpolated using a Gaussian filter.

In the filtering stage the Fourier Spectrum of each block is filtered with a Log-Gabor (introduced by [14]) which is tuned to its local orientation and frequency. Furthermore, experiments showed that a bandwidth of three times the variance of the Fourier Spectrum and as spread value the blocksize/4 are well suited for filtering. By using the fast inverse Fourier transform the filtered Fourier Spectra are utilized as new block values. Boundary effects are reduced by using half-overlapping blocks. An exemplary result of the registration & enhancement procedure is depicted in Fig. 1.

2.2. Cross-section code computation & matching

As suggested in [9] a Gabor filterbank is used to extract annual ring pattern features. Because of the constant ridge frequencies in human fingerprints a single Gabor filter and its rotated versions are sufficient. The frequencies of annual ring patterns are strongly varying and thus different Gabor filters are required to capture additional information from the annual ring frequencies in different orientations. For a CS image width of 512 pixels six different Gabor filters are suggested. For each Gabor filter eight rotated versions are created. Consequently, the Gabor filterbank consists of 48 filters.

The CS-Code computation is performed in three stages. In the first stage the enhanced input image is filtered with each filter in the filterbank. Each filtered image is subdivided into blocks (e.g. 32x32 pixels). For all blocks the absolute deviations of the gray values are computed. The absolute deviations of each image are stored into a matrix, which can be denoted as Standard Deviation Map (Stdev Map). In the middle of Fig. 1, the filtering and Stdev map computation procedure is illustrated. Altogether 48 Stdev Maps are computed and stored as one-dimensional vectors in a CSV file.

Rotational variances are compensated by repeatedly computing features for rotated versions of the input image. Compared to fingerprints, the rotational misalignment range of a CS image is not restricted to a certain range. One strategy to solve this issue, is to perform rotational pre-alignment in the registration & enhancement stage to restrict the misalignment range. For the utilized testset in our experiments the misalignment range lies between $-15°$ to $15°$. As shown in Fig. 1 for each input image a set of CS-Codes $(rot_{-15}, ..., rot_0, ..., rot_{15})$ is computed.

Matching is performed by computing the minimum matching score between all CS-Codes from two CS images. The matching score between to CS-Codes can be computed with a set of distance metrics. Two bin-by-bin distances (L1-Norm - L_1, L2-Norm - L_2), one cross-bin distance (EMD -

see [15]) and a simple 2D-matching distance are examined. The 2D-matching distance computes for each block the average L_1 distance between its Stdev value and the Stdev values of all adjacent blocks.

3. EXPERIMENTS AND RESULTS

In the experimental evaluation temporal and longitudinal variances are analysed using a testset of 35 CS slices from a single tree log. The first experiment assesses the temporal variances between time-delayed captured images from equal CSs. In the second experiment longitudinal variances between different CSs along the longitudinal axis of tree logs are assessed.

Testset: The 35 CS slices are from two sections which were cut from one spruce tree log with a spacing of approximately three centimetres. 18 slices were cut from the first and 17 slices from the second section. The slices were cut with a bandsaw and the thickness of the slices is approximately two centimetres. Each slice was captured four times (Canon EOS 5D Mark II) with different time spans between each capturing session. For the last session, the slices were stored in a balanced climate of 21° and 60% humidity. All images were captured under equal light conditions in a photo studio. For a constant rotational alignment between different sessions pins were utilized as position markers. The distance between the CS slice and the camera was fixated using a tripod. In Fig. 2 the four images of Slice #10 are illustrated. Additionally, for all images the CS borders and pith positions were manually marked and are available as xy-coordinates.

Fig. 2: Testset example: Slice #10 - Section 2 / Sessions 1-4

Computational details: For each of the four images from each CS slice 31 CS-Codes $(rot_{-15}, ..., rot_0, ..., rot_{15})$ are computed. In the registration & enhancement stage the rotated CSs are scaled to 512 pixels in width and for enhancement 32x32 half-overlapping pixels blocks are utilized. The CS-Codes are computed using 16x16 non-overlapping blocks for the Stdev maps. The utilized Gabor filterbank is build up on six different Gabor filters tuned to 8 directions:

$$G(\lambda, \theta, \sigma, \gamma) = G(\lambda, \sigma) =$$
$$((2.5, 2), (2.5, 2), (3.5, 3), (4.5, 3), (5.5, 3), (6.5, 3)),$$
$$\theta = \{0, 22.5, ..., 135, 157.5\}, \gamma = 0.7$$

In addition to the 31 CS-Codes of each CS slice, further seven CS-Codes $(rot_{45}, rot_{90}, ..., rot_{270}, rot_{315})$ were computed. These rotations are not in the expected misalignment range considered in the matching procedure. Thus, these CS-Codes are utilized to simulate a set of CS-Codes descending from different tree logs, i.e. used to simulate interclass variances.

Subsequently, three different variances are computed. Temporal variances are the matching scores among the CS-Codes of the four different session images from one CS slice. Longitudinal variances are computed among the CS-Codes of the images from each session. Finally, interclass variances are computed among the CS-Codes as described above. The CS-Code framework and the experiments are implemented in JAVA.

3.1. Results

The results are assessed in two stages. For each distance metric and the different variances, the corresponding matching score distributions (SDs) are computed. Note that these correspond to genuine and impostor distributions in biometrics [16]. First, the intersections between the SDs of the temporal, longitudinal and interclass variances for the different distances metric are evaluated. Subsequently, we analyse the temporal and longitudinal variances of the best distance metric.

SD intersection analysis: According to the percent of intersection between the temporal, longitudinal and interclass SDs the best distance metric is determined. Thereby, the intersections between the temporal/ longitudinal SDs and the interclass-SD are used as main evaluation criteria. The lower the overlap between those SDs, the more suitable is the distance metric to distinguish between CS-Codes from different tree logs. In case of a real world application a high percentage of intersection between the temporal and longitudinal SDs is very important. Only then a biometric system is robust to temporal and longitudinal variances. In Table 1 the percentages

Distance Metric	Temp-Long	Temp-Inter	Long-Inter
EMD	82.25%	24.66%	33.00%
L_1	68.51%	1.31%	6.00%
L_2	72.10%	3.77%	14.00%
2D-matching	67.53%	2.86%	13.00%

Table 1: Intersections of the score distributions (SDs)

of intersections between the SDs for all evaluated distance metrics are listed. The lowest overlaps between the temporal/ longitudinal SDs and the interclass SD are reached using the L_1 norm (see Fig. 3a). Using the L_1 norm, there is an overlap of 1.31% between the temporal and the interclass SD. Furthermore, the overlap between the longitudinal and interclass SD is very low and accounts 6%. Although, the interclass variances are generated using the the same testset the low overlaps between the temporal/longitudinal SDs and the interclass SD indicate that it is possible to separate CS-Codes computed from different tree logs. Considering the temporal and longitudinal SDs, it is a bit surprising that the overlaps are very high. In this regard, a detailed analysis of the temporal and longitudinal SDs brings some interesting insights as follows.

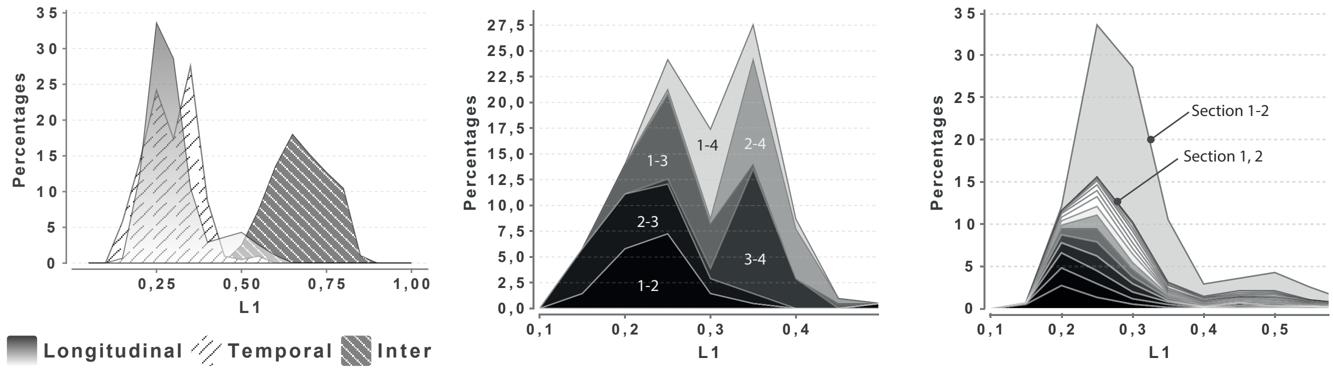

(a) Matching score distributions

(b) Temporal SD - stacked session subset chart

(c) Longitudinal SD - stacked distance subset chart

Fig. 3: Temporal/longitudinal and interclass score distribution (SD) analysis

Temporal variances: In Fig. 3b the subset structure of the temporal SD (L_1 norm) is illustrated. The labelled subset areas in the chart illustrate the proportions of the matching scores between different sessions and are stacked one above the other. The labels specify the indexes of the sessions used to compute the matching scores. Overall, the highest CS-Code distances arise in subsets where one session is compared to Session #4. This results from storing the CSs in a balanced climate between Sessions #3 and #4. This caused remarkable visual changes. Due to the decreasing moisture content, the contrast and intensity of the annual ring pattern changes and cracks as well as discolourations arise. As expected, the lowest CS-Code distances are computed between Sessions 1-2 and 2-3. All in all, the results indicate that an increasing time span between two images of the same CS deteriorates the CS-Code distance.

Longitudinal variances: Finally, the longitudinal variances (L_1 norm) are assessed. It can be assumed that with an increasing longitudinal distance between two CS slices the CS-Code distance increases too. The chart in Fig. 4 illustrates the mean matching scores for different slice distances grouped session-wise. For each session the mean CS-Code distances increase with an increasing slice distance. Lastly, the chart in Fig. 3c illustrates different subsets of the longitudinal SD. The largest subset labelled "Section 1-2" contains all matching scores between all slices from the first tree section to all slices from the second section. In this particular case, the slice distances range between 1 to 35 slices. The second subset "Section 1,2" contains all matching scores between the slices of the two sections. As in Fig. 4, this subset is further subdivided into subsets according to the slice distance of the compared slices. The bottom subset area contains all matching scores with slice distance 1. From bottom up the slice distance increases. Considering the subset peaks, the chart illustrates that with an increasing slice distance the CS-Code distances shift remarkable to higher values.

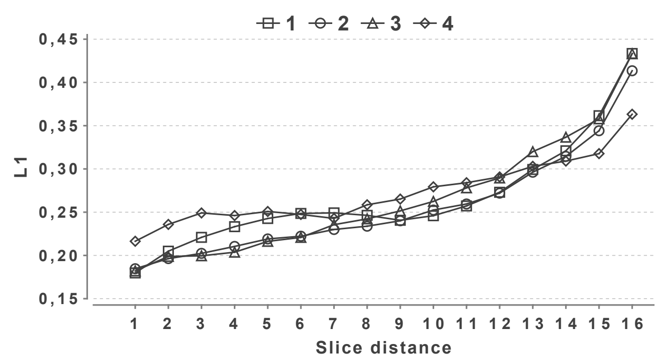

Fig. 4: Longitudinal variances - matching score analysis

4. CONCLUSION

In conclusion it can be stated that preliminary expectations about longitudinal and temporal variances of CSs of tree logs are confirmed by the results of our experiments. In this work Gabor-features of CS slice images of a tree log are computed and compared with respect to the temporal and longitudinal variances. These variances are related to the robustness of biometric log traceability using log end images. Results show that with an increasing time span between two images of the same CS the CS-Code distance increase too. Furthermore, it is shown that adjacent CS slices show low CS-Code distances and with an increasing slice distance the CS-Code distances increase. Finally, our results indicate that biometric systems using log end images are able to overcome issues caused by environmental influences and log length cutting or capturing different log ends.

In future work more matured features should be extracted and the performance of a biometric log recognition framework using a real world testset should be assessed.

5. REFERENCES

[1] Dennis P. Dykstra, George Kuru, Rodney Taylor, Ruth Nussbaum, William B. Magrath, and Jane Story, "Technologies for wood tracking," Tech. Rep., World Bank - WWF Alliance report, 2003.

[2] S. Korten and C. Kaul, "Application of RFID (Radio frequency identification) in the timber supply chain," *Croatian Journal of Forest Engineering*, vol. 29, no. 1, 2008.

[3] I. Ehrhardt, H. Seidel, and N. Doden, "Potentials for savings by implementing rfid and telematic technologies in the timber and biomass supply chain," in *In Procs. of the International Conference on Biosystems Engineering*, Tartu, EST, 2010, vol. 8, pp. 47–59.

[4] S. Chiorescu and A. Grönlund, "The fingerprint approach: using data generated by a 2-axis log scanner to accomplish traceability in the sawmill's log yard," *Forest Products Journal*, vol. 53, pp. 78–86, 2003.

[5] S. Chiorescu and A. Grönlund, "The fingerprint method: Using over-bark and under-bark log measurement data generated by three-dimensional log scanners in combination with radiofrequency identification tags to achieve traceability in the log yard at the sawmill," *Scandinavian Journal of Forest Research*, vol. 19, no. 4, pp. 374–383, 2004.

[6] Jens Flodin, Johan Oja, and Anders Grönlund, "Fingerprint traceability of sawn products using x-ray log scanning and sawn timber surface scanning," in *Proccedings of Quality control for wood and wood products: COST Action E 53 the first conference*, 2007.

[7] Jens Flodin, Johan Oja, and Anders Grönlund, "Fingerprint traceability of logs using the outer shape and the tracheid effect," *Forest Products Journal*, vol. 58, no. 4, pp. 21–27, 2008.

[8] J. Flodin, J. Oja, and J. Grönlund, "Fingerprint traceability of sawn products using industrial measurement systems for x-ray log scanning and sawn timber surface scanning," *Forest Products Journal*, vol. 58, pp. 11, 2008.

[9] A. K. Jain, S. Prabhakar, L. Hong, and S. Pankanti, "Filterbank-based fingerprint matching," *IEEE Transactions on Image Processing*, vol. 9, no. 5, pp. 846–859, May 2000.

[10] A. Jain, A. Ross, and S. Prabhakar, "Fingerprint matching using minutiae and texture features," in *Procs. of the International Conference on Image Processing (ICIP'01)*, Thessaloniki, GR, 2001, vol. 3, pp. 282–285.

[11] Lin Hong, Yifei Wan, and Anil Jain, "Fingerprint image enhancement: Algorithm and performance evaluation," *IEEE Trans. Pattern Anal. Mach. Intell.*, vol. 20, no. 8, pp. 777–789, Aug. 1998.

[12] R. Schraml and A. Uhl, "Pith estimation on rough log end images using local fourier spectrum analysis," in *Proceedings of the 14th Conference on Computer Graphics and Imaging (CGIM'13)*, Innsbruck, AUT, Feb. 2013.

[13] Kristin Norell and Gunilla Borgefors, "Estimation of pith position in untreated log ends in sawmill environments," *Computers and Electronics in Agriculture*, vol. 63, no. 2, pp. 155–167, 2008.

[14] H. Knutsson and G. H. Granlund, "Texture analysis using two-dimensional quadrature filters," in *IEEE Computer Society Workshop on Computer Architecture for Pattern Analysis and Image Database Management*, Pasadena, USA, 1983.

[15] Y. Rubner, C. Tomasi, and L.J. Guibas, "A metric for distributions with applications to image databases," in *Computer Vision, 1998. Sixth International Conference on*, 1998, pp. 59–66.

[16] D. Maltoni, D. Maio, A. K Jain, and S. Prabhakar, *Handbook of fingerprint recognition*, Springer New York, 2009.